RESEARCH ARTICLE | NOVEMBER 19 2024

Tunable ultrabroadband hybrid terahertz emitter combining a spintronic and a GaSe source

Afnan Alostaz ; Oliver Gueckstock ; Junwei Tong ; Jana Kredl ; Chihun In ; Markus Münzenberg; Claus M. Schneider ; Tobias Kampfrath ; Tom S. Seifert

Appl. Phys. Lett. 125, 212402 (2024)
https://doi.org/10.1063/5.0226564

Applied Physics Letters ARTICLE pubs.aip.org/aip/apl

Tunable ultrabroadband hybrid terahertz emitter combining a spintronic and a GaSe source

Cite as: Appl. Phys. Lett. **125**, 212402 (2024); doi: 10.1063/5.0226564
Submitted: 2 July 2024 · Accepted: 24 September 2024 ·
Published Online: 19 November 2024

Afnan Alostaz,[1,2,3,a] Oliver Gueckstock,[1] Junwei Tong,[1] Jana Kredl,[4] Chihun In,[1] Markus Münzenberg,[4] Claus M. Schneider,[2] Tobias Kampfrath,[1,3] and Tom S. Seifert[1,a]

AFFILIATIONS

[1]Department of Physics, Freie Universität Berlin, 14195 Berlin, Germany
[2]Peter Grünber Institut (PGI-6), Forschungszentrum Jülich GmbH, D-52425 Jülich, Germany
[3]Department of Physical Chemistry, Fritz Haber Institute of the Max Planck Society, 14195 Berlin, Germany
[4]Institut für Physik, Universität Greifswald, 17489 Greifswald, Germany

[a]**Authors to whom correspondence should be addressed:** afnan.alostaz@fu-berlin.de and tom.seifert@fu-berlin.de

ABSTRACT

Terahertz (THz) time-domain spectroscopy (TDS) is a sensitive approach to material characterization. It critically relies on a sufficiently large bandwidth, which is not straightforwardly available in typical THz-TDS systems that are often limited to below 3 THz. Here, we introduce a hybrid THz-source concept based on a spintronic THz emitter (STE) deposited onto a thin, free-standing GaSe nonlinear crystal. By tuning the magnetic state and the phase-matching parameters of the hybrid emitter, we generate an ultrabroadband spectrum covering the full range from 1 to 40 THz. We achieve significantly enhanced spectral amplitudes above 10 THz compared to the bare STE, resulting in ultrashort THz-pulse durations down to 32 fs. Finally, we demonstrate the straightforward tunability of the shape of the few-cycle pulse from symmetric to antisymmetric.

Terahertz (THz) radiation is a sensitive probe of many low-energy excitations in solids, liquids, and gases.[1] Prominent examples in condensed matter include crystal-lattice vibrations, spin waves, and intraband electron transport. The sensitivity to these resonances enables broad potential applications of linear THz spectroscopy, e.g., identification of materials,[2] thickness determination of thin layers of, e.g., polymers[3] or paints,[4] and the measurement of water content in plants.[5]

Importantly, for those tasks, THz time-domain spectroscopy (THz-TDS) is ideally suited as it allows one to record the signal amplitude and phase simultaneously.[2] For THz-pulse generation, THz-TDS systems driven by nanojoule-class femtosecond laser pulses often use optical rectification in nonlinear crystals, such as GaP, ZnTe, and GaSe, or photoconductive switches.[1,6] Typically, these sources work in relatively narrow frequency ranges that are limited by phase-matching conditions or phonon-related attenuation bands typically in the range 5–10 THz.[7] Accordingly, linear THz-spectroscopic measurements are common in the range 1–5 THz for ZnTe and GaP crystals as well as for photoconductive emitters,[2] or at 10–40 THz for GaSe crystals.[8]

Recently, ultrabroadband spintronic THz emitters (STEs) emerged as a promising THz-emitter platform that, in particular, covers the range 1–15 THz.[9,10] STEs are based on thin metallic multilayers (Fig. 1). Following excitation by a femtosecond laser pulse, an out-of-plane spin current j_s from a ferromagnetic-metal layer F propagates into adjacent nonferromagnetic-metal layers N, in which j_s is converted into an in-plane charge current j_c. The latter radiates an electromagnetic pulse with THz frequencies into the optical far-field. STEs are insensitive to the pump wavelength,[11] and the polarization plane of the emitted THz pulse can easily be set by the F magnetization at kilohertz rates.[12] The STE's ability to generate ultrabroadband THz pulses covering the entire THz range led to detailed insight into, e.g., the THz refractive index of a polymer[10] or transverse THz magnetotransport in magnetic metals.[8]

To extend the bandwidth of the STE, Chen *et al.*[13] combined it with a semiconducting material, resulting in an enhanced performance in the frequency range 0.1–0.5 THz by 2–3 orders of magnitude compared to a standard STE, as shown in Fig. 1. However, while STEs can excellently cover the interval 1–15 THz, which includes the THz gap at 5–10 THz, the spectral amplitude above 15 THz decreases rapidly. A

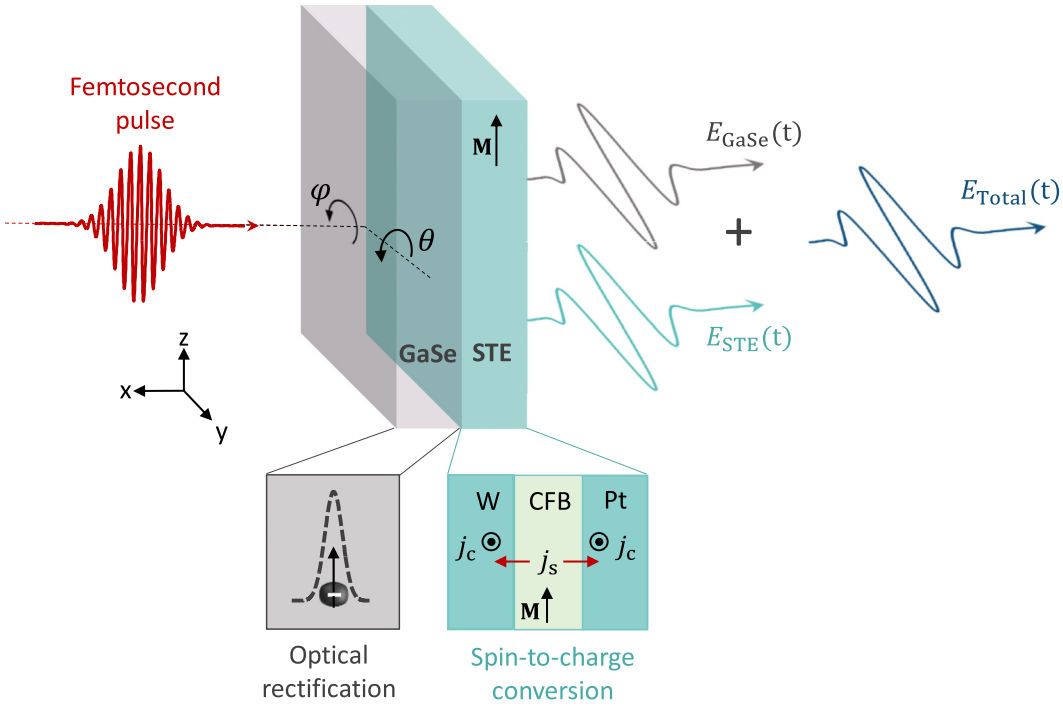

FIG. 1. Hybrid THz emitter concept. The emitter consists of a thin GaSe crystal with a spintronic THz emitter (STE) grown on top that has an in-plane magnetization **M**. Upon excitation by a femtosecond near-infrared laser pulse, optical rectification inside the GaSe crystal generates a THz pulse with electric field $E_{GaSe}(t)$ vs time t (grey). The STE thin-film stack consists of a metallic ferromagnetic CoFeB (CFB) layer F and two layers made of nonferromagnetic metals (W, Pt). After optical excitation, a spin current j_s is injected from F into the adjacent W and Pt layers. Spin–orbit interaction converts j_s into an in-plane charge current j_c that leads to the emission of a THz pulse with field $E_{STE}(t)$(green). Both THz electric fields add up to the total emitted THz pulse with electric field $E_{Total}(t)$ (blue). The azimuthal angle of the emitter is φ, and its tilt angle relative to the direction of the incident pump beam is θ. The STE magnetization **M** is independent of φ, but tilts with θ. We detect the THz-field component polarized perpendicular to the plane of incidence and **M**, i.e., along the y direction.

boost of these high-frequency components could strongly reduce acquisition times in linear THz-TDS measurements and produce ultrashort THz pulses that are well suited as probe pulses in experiments as diverse as transient THz-conductivity measurements,[14] THz pump photoelectron–probe experiments[15] or THz field-driven scanning tunneling microscopy.[16]

Here, we present a hybrid THz emitter based on a free-standing GaSe crystal, on top of which an STE is deposited (see Fig. 1). The basic idea of the hybrid emitter relies on superimposing the generated THz pulses from the STE and GaSe. Importantly, the phase-matching conditions and the angular dependence of the nonlinear coefficient in GaSe allow for tuning its emission through the angle of incidence, the polarization of the pump beam and the sample azimuth.[17] Along with the polarity of the STE pulse, which can be set by an external magnetic field, one can tune the resulting superimposed THz pulse in duration and shape. In this way, we generate THz pulses that cover the full range of 1–40 THz with enhanced spectral amplitudes above 10 THz compared to the bare STE. We achieve shortest THz pulse durations of only 32 fs and tune the waveform shape from symmetric to antisymmetric by simply reversing the external magnetic field.

Our hybrid emitter consists of a free-standing GaSe crystal (z-cut, diameter of 4 mm) with a thickness of 30 μm, on top of which a STE with stacking order W(2 nm)|$Co_{40}Fe_{40}B_{20}$(1.8 nm)|Pt(2 nm) is deposited (see the supplementary material). The in-plane sample magnetization **M** is saturated by a static external magnetic field of about 40 mT (Fig. 1).

In the experiment, the near-infrared pump pulse (duration 10 fs, central wavelength 800 nm, repetition rate 80 MHz, pulse energy 5 nJ, spot radius at $1/e^2$ of the intensity of around 25 μm, and a fluence of up to 0.18 mJ/cm^2) is incident from the GaSe. Further details about the experimental setup can be found in the supplementary material (Fig. S1) and in Ref. 10. Pumping from the STE side instead from the GaSe side results in a suppression of high THz frequencies generated in GaSe (see Fig. S2) due to a loss of pump energy before exciting the GaSe. The sample can be rotated about the sample normal (azimuth angle φ) and the y-axis (angle of incidence θ of the pump). The starting azimuth of $\varphi = 0°$ is chosen by setting GaSe to its minimum THz emission under normal incidence with $\theta = 0°$ (see Fig. 1). The sample magnetization is along the z-axis such that the charge currents inside the STE run along the y-axis, thereby ensuring equal THz outcoupling efficiency upon varying θ.

To detect the generated p-polarized (along y-axis) THz pulses $S^{\pm}(t)$ for opposite STE magnetizations $\pm$**M**, we use electro-optic sampling[18] in a 250 μm thick GaP(110) crystal with probe pulses (1 nJ energy) from the same laser. All experiments are performed under a dry-air atmosphere.

To extract the THz electric field $E(t)$ at the detector position, we use an inversion procedure that is based on deconvolution of the

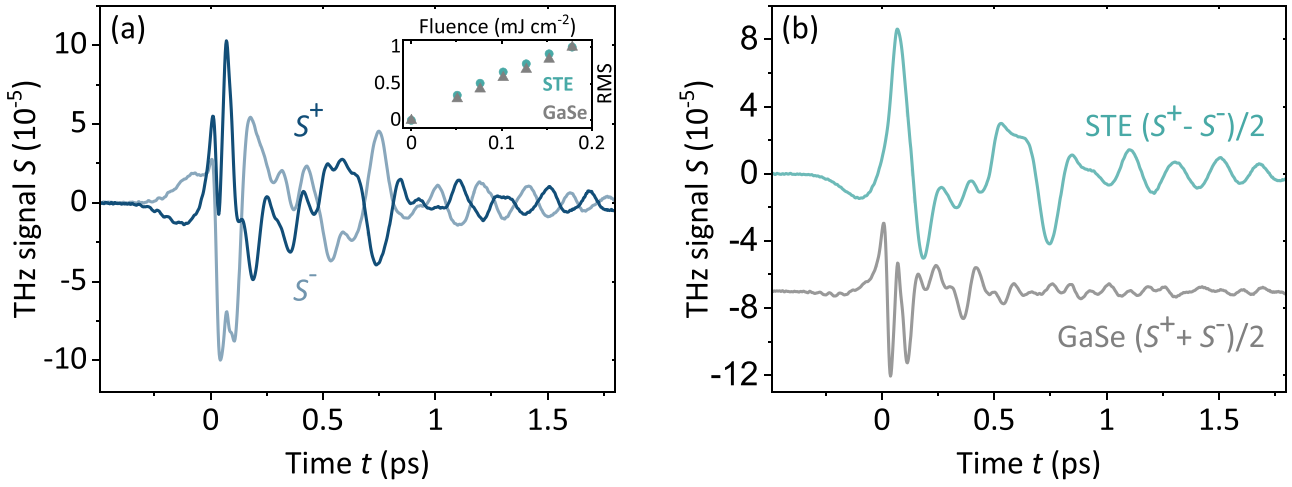

FIG. 2. Raw THz emission signals from the hybrid emitter. (a) Electro-optic signals $S^{\pm}(t)$ vs time t of the THz field emitted from the hybrid emitter for magnetization directions $\pm\mathbf{M}$. Signals refer to the field component perpendicular to the in-plane sample magnetization $\mathbf{M}$. The inset shows the root mean square (RMS) of the THz emission signal vs the pump fluence. (b) Signal components even and odd in $\mathbf{M}$, i.e., $(S^+ \pm S^-)/2$. The two signals represent the signals from the GaSe and STE emitter, respectively. The GaSe signal is vertically offset for clarity.

response function $H = H(t)$ of the GaP detection crystal from the detected THz signals $S(t)$, i.e., by solving $S = H * E$ for $E = E(t)$.[19,20]

To determine the duration of the THz pulse, we first calculate the intensity envelope $|A(t)|^2$, where the complex-valued field $A(t) = (\mathcal{H}E)(t)$ of the THz pulse is given by the Hilbert transformation $\mathcal{H}$ of E. Second, we calculate the temporal width Δt of $|A(t)|^2$ as the standard deviation for a restricted time window (see Fig. S3) around the main THz signal by[21]

$$\Delta t = \sqrt{\langle t^2 \rangle - \langle t \rangle^2}, \tag{1}$$

where

$$\langle t^n \rangle = \frac{\int_{-\infty}^{\infty} \mathrm{d}t\, t^n |A(t)|^2}{\int_{-\infty}^{\infty} \mathrm{d}t\, |A(t)|^2}. \tag{2}$$

Further details about the pulse-duration calculations with respect to the amplitude envelope $|A(t)|$ instead of the intensity envelope $|A(t)|^2$ and the corresponding two-dimensional color maps of the amplitude-envelope pulse duration are given in the supplementary material (see Figs. S4 and S5).

Figure 2(a) shows raw THz emission signals $S^{\pm}(t)$ from the hybrid emitter under normal incidence ($\theta = 0°$), with a linear pump polarization of 45° and at an azimuth of $\varphi = 30°$. Upon reversing the sample magnetization from $+\mathbf{M}$ to $-\mathbf{M}$, distinct changes in the THz waveform appear. We extract the GaSe and STE contributions to the THz waveform by adding and subtracting the waveforms for $\pm\mathbf{M}$, respectively [Fig. 2(b)]. Indeed, this procedure yields two waveforms $[S^+(t) \pm S^-(t)]/2$, which show distinct dynamics, reminiscent of typical GaSe (sum, faster dynamics) and STE (difference, slower dynamics) THz emission signals.[10,17] The inset in Fig. 2(a) confirms that our THz source works in the linear fluence regime under the conditions of our

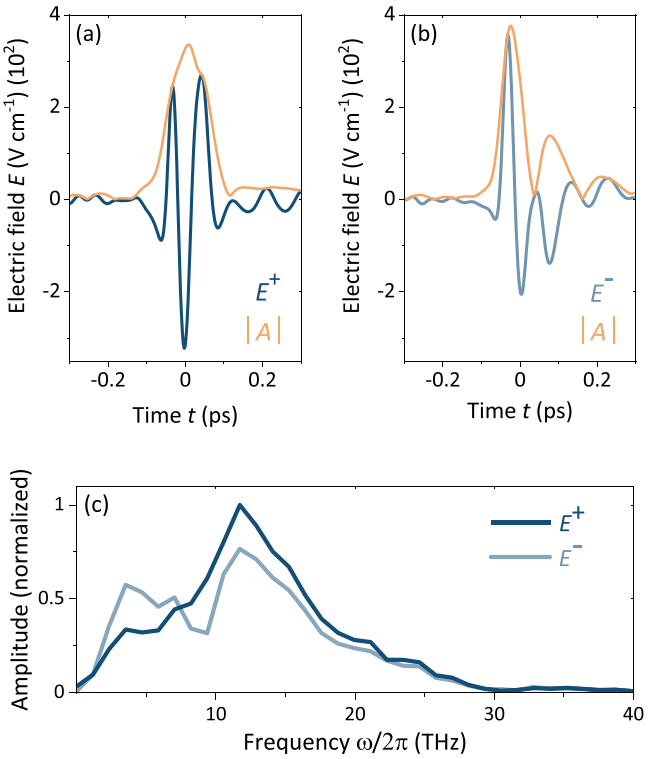

FIG. 3. Extracted THz-electric-field traces from the hybrid emitter. (a) Terahertz electric field $E^+(t)$ in the detection focus as retrieved from the corresponding THz signals for an angle of incidence of $\theta = 0°$ (see Fig. 1) and an azimuthal angle $\varphi = 30°$ for magnetization $+\mathbf{M}$ and (b) $E^-(t)$ for magnetization $-\mathbf{M}$. (c) THz spectra obtained by Fourier transformation of the corresponding field traces in panels (a) and (b). Both spectra are normalized by the maximum amplitude of the signal E^+.

experiment. These findings highlight the general feasibility of our hybrid emitter concept.

Figure 3 displays the extracted THz electric field $E^{\pm}(t)$ incident onto the electro-optic detector. To bridge spectral regions in the numerical electric-field extraction, where the electro-optic detector response reaches zero, i.e., at around 8 THz (Fig. S6), we perform a linear interpolation in the frequency domain. The resulting THz electric field reaches peak strengths of about 400 V/cm in the detection focus. The retrieved signal envelopes [Figs. 3(a) and 3(b)] for opposite sample magnetizations demonstrate the tunability of the hybrid emitter by constructive or destructive superposition of the STE and GaSe THz pulses. The related Fourier spectra indicate that frequencies up to about 40 THz can be covered [Fig. 3(c)].

Based on these findings, we optimize the THz pulse from the hybrid emitter by variation of its tilt angle θ and azimuth φ. Specifically, Fig. 4 displays the pulse duration $\Delta t(\theta, \varphi)$ of the total THz electric field at the detector position vs (θ, φ) in two-dimensional color maps not only for magnetization directions $+\mathbf{M}$ [Fig. 4(a)] and $-\mathbf{M}$ [Fig. 4(b)] but also for the field from the STE [Fig. 4(c)] and the GaSe part [Fig. 4(d)] of the hybrid emitter. Ideally, the values $\Delta t(\theta, \varphi)$ for $+\mathbf{M}$ and $\varphi = 0°$–$60°$ should mirror those for $-\mathbf{M}$ and $\varphi = 60°$–$120°$ due to the expected sign change of the GaSe component of the THz electric field. Overall, our data confirm this expectation, whereas minor deviations are ascribed to emitter heterogeneities.

Figure 5 shows the result of our optimization procedure. Remarkably, we obtain an ultrashort THz electric field with an intensity-envelope duration of down to 32 fs [Fig. 5(a)] and an ultrabroad spectrum [Fig. 5(b)]. It is achieved for $\theta = 40°$ and $\varphi = 30°$ in the $+\mathbf{M}$ configuration.

We conclude that our hybrid emitter unifies the advantages of the STE and GaSe emitters within one device, where the STE and GaSe, respectively, cover the range 1–10 THz and 10–40 THz efficiently [Fig. 5(b)]. A relative comparison between the THz signals from the hybrid emitter and an STE on a sapphire substrate as well as a bare GaSe crystal is provided in the supplementary material (Fig. S7).

Further tuning of THz electric fields under the shortest pulse conditions is achieved by exciting the hybrid emitter with circularly polarized light. By changing the helicity of the pump radiation from left- to right-handed, a phase shift of $\pm 90°$ can be obtained for the GaSe-related THz-emission signal. This mode reveals the potential for even shorter pulse durations compared to excitation with 45° linear pump polarization (Fig. S8).

Eventually, we demonstrate tuning of the THz pulse shape from symmetric to antisymmetric by reversing the direction of the STE

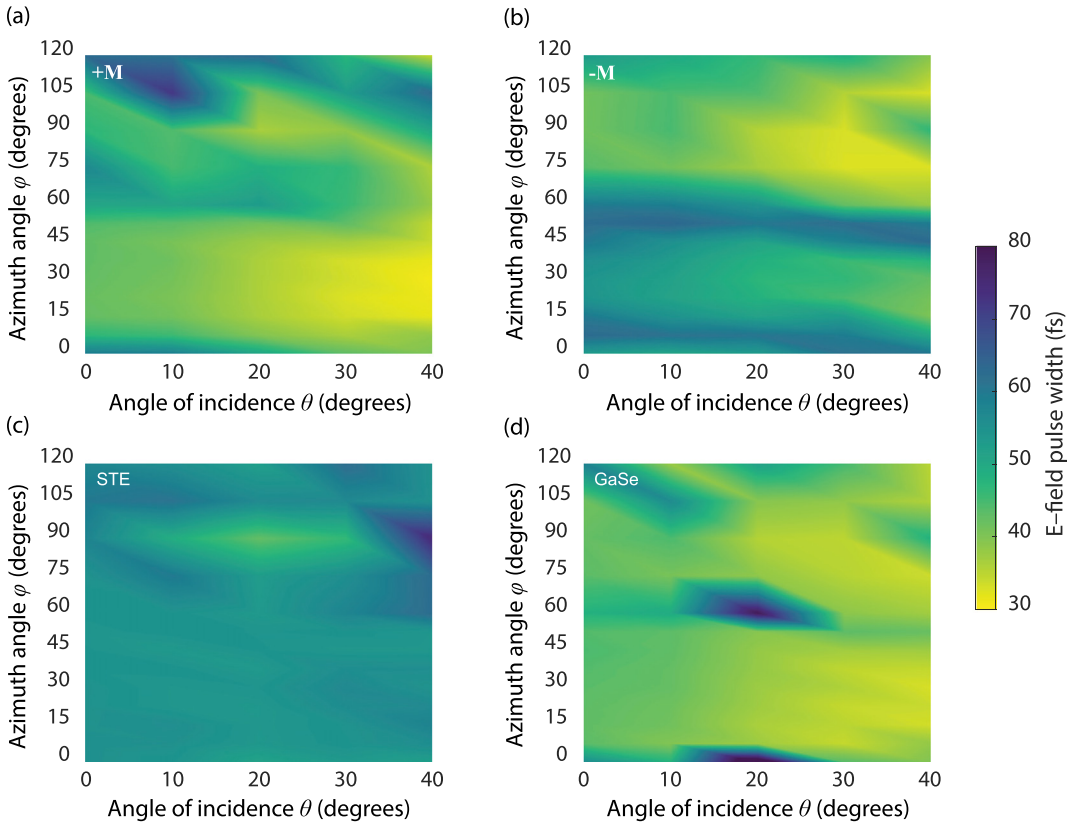

FIG. 4. THz pulse duration $\Delta t(\theta, \varphi)$ [Eq. (2)] vs tilt angle θ and azimuthal angle φ of the hybrid emitter. (a) Measured map $\Delta t(\theta, \varphi)$ for STE magnetization $+\mathbf{M}$ and (b) $-\mathbf{M}$. The shortest pulse duration is obtained for $(\theta, \varphi) \approx (40°, 30°)$ and $+\mathbf{M}$. (c) Duration $\Delta t(\theta, \varphi)$ of the pulse from the STE and (d) GaSe part of the hybrid emitter.

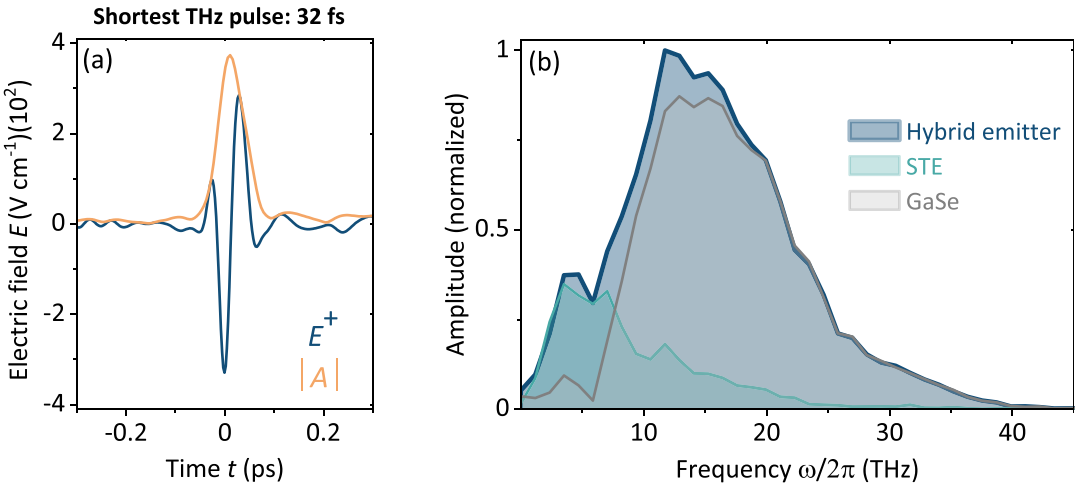

FIG. 5. Optimized THz-electric-field transient from the hybrid emitter. (a) Extracted THz electric field $E^{+}(t)$ of the shortest pulse with a duration of 32 fs with respect to the intensity envelope $|A(t)|^2$ [see Eq. (2)]. The parameters of the hybrid THz emitter are $\theta = 40°$, $\varphi = 30°$, and $+\mathbf{M}$ magnetization. The linear pump polarization was set to 45°. (b) Amplitude spectrum of the pulse in panel (a) together with the respective contributions of the STE and the GaSe crystal, normalized to the maximum spectral amplitude of the hybrid emitter spectrum.

magnetization from $+\mathbf{M}$ [Fig. 6(a)] to $-\mathbf{M}$ [Fig. 6(b)], while maintaining the ultrashort THz pulse duration. This result paves the way toward ultrabroadband applications that are sensitive to the THz pulse shape, e.g., THz-streaking of electron beams,[22] THz-driven scanning tunneling microscopy,[23] or THz high-harmonic generation.[24]

In summary, we introduce a hybrid-emitter concept that unifies the benefits of STEs and GaSe crystals as THz emitters in one device. Their combination results in an ultrabroadband THz source that remarkably covers the range from 1 to 40 THz with strongly enhanced spectral amplitudes above 10 THz compared to the bare STE. The resulting THz pulses feature a pulse duration down to 32 fs, which makes them prime candidates for experiments probing ultrafast dynamics of diverse types of THz resonances in all phases of matter.

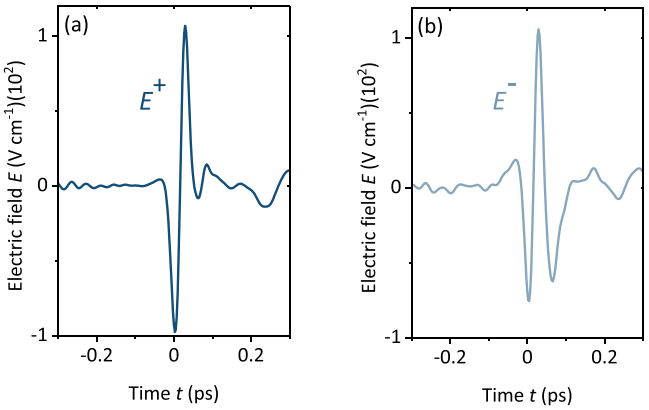

FIG. 6. Tuning from antisymmetric to symmetric THz pulse shapes. (a) Electric field $E^{+}(t)$ of the THz pulse incident on the detector for magnetization $+\mathbf{M}$ and (b) the field $E^{-}(t)$ for magnetization $-\mathbf{M}$. The magnetization direction permits tuning from a symmetric [sine-like, panel (a)] to an antisymmetric [cosine-like, panel (b)] pulse shape. The emitter settings are $\theta = 30°$ and $\varphi = 120°$.

We note that a future optimization of the heat dissipation in our hybrid emitter by, for instance, contacting it to a thicker substrate, could further boost the THz field amplitude. We expect an increase of about a factor of 10 in the THz field under similar excitation conditions from a comparison to STEs grown on a 500-μm-thick sapphire substrate (Fig. S7).[10]

See the supplementary material for further details on the experiments.

The authors thank Genaro Bierhance (FU Berlin) for fruitful discussions. This work was supported by the Federal Ministry of Education and Research of Germany in the framework of the Palestinian-German Science Bridge (BMBF Grant No. 01DH16027). Open-access funding is enabled and organized by Projekt DEAL. TK and TSS acknowledge funding by the German Research Foundation through the collaborative research center TRR 227 "Ultrafast spin dynamics" (project ID 328545488, projects A05 and B02) and the priority program INTEREST (project ITISA, project No. KA 3305/5-1).

AUTHOR DECLARATIONS

Conflict of Interest

The authors have no conflicts to disclose.

Author Contributions

Afnan Alostaz: Conceptualization (equal); Data curation (lead); Formal analysis (lead); Methodology (equal); Visualization (lead); Writing – original draft (lead); Writing – review & editing (lead). **Oliver Gueckstock:** Conceptualization (supporting); Data curation (supporting); Methodology (supporting); Visualization (supporting); Writing – review & editing (supporting). **Junwei Tong:** Conceptualization (supporting); Data curation (supporting); Methodology (supporting);

Validation (supporting); Visualization (supporting). **Jana Kredl:** Resources (lead); Writing – review & editing (supporting). **Chihun In:** Data curation (supporting); Methodology (supporting); Writing – review & editing (supporting). **Markus Münzenberg:** Resources (lead); Writing – review & editing (supporting). **Claus M. Schneider:** Validation (supporting); Visualization (supporting). **Tobias Kampfrath:** Conceptualization (equal); Formal analysis (supporting); Methodology (equal); Validation (equal); Writing – review & editing (equal). **Tom S. Seifert:** Conceptualization (lead); Data curation (supporting); Formal analysis (equal); Methodology (lead); Resources (supporting); Validation (supporting); Visualization (supporting); Writing – original draft (lead); Writing – review & editing (lead).

DATA AVAILABILITY

The data from the main text figures of this article are avialable on the repository Zenodo (https://zenodo.org/records/13936518), Ref. 25. Further data are available from the corresponding authors upon reasonable request.

REFERENCES

[1]M. Koch, D. M. Mittleman, J. Ornik, and E. Castro-Camus, Nat. Rev. Methods Primers **3**(1), 48 (2023).
[2]J. Neu and C. A. Schmuttenmaer, J. Appl. Phys. **124**(23), 231101 (2018).
[3]S. Wietzke, C. Jansen, M. Reuter, T. Jung, D. Kraft, S. Chatterjee, B. Fischer, and M. Koch, J. Mol. Struct. **1006**(1–3), 41 (2011).
[4]F. Ellrich, M. Bauer, N. Schreiner, A. Keil, T. Pfeiffer, J. Klier, S. Weber, J. Jonuscheit, F. Friederich, and D. Molter, J. Infrared. Millimeter, Terahertz Waves **41**(4), 470 (2020).
[5]J. Iriarte, D. Etayo, I. Palacios, I. Maestrojuan, I. Liberal, A. Rebollo, J. Teniente, I. Ederra, and R. Gonzalo, presented at the Proceedings of the 5th European Conference on Antennas and Propagation (EUCAP), 2011.
[6]C. W. Berry, N. Wang, M. R. Hashemi, M. Unlu, and M. Jarrahi, Nat. Commun. **4**(1), 1622 (2013).
[7]T. Kampfrath, J. Nötzold, and M. Wolf, Appl. Phys. Lett. **90**(23), 231113 (2007).
[8]T. S. Seifert, U. Martens, F. Radu, M. Ribow, M. Berritta, L. Nádvorník, R. Starke, T. Jungwirth, M. Wolf, I. Radu, M. Münzenberg, P. M. Oppeneer, G. Woltersdorf, and T. Kampfrath, Adv. Mater. **33**(14), 2007398 (2021).
[9]T. S. Seifert, L. Cheng, Z. Wei, T. Kampfrath, and J. Qi, Appl. Phys. Lett. **120**(18), 180401 (2022).
[10]T. Seifert, S. Jaiswal, U. Martens, J. Hannegan, L. Braun, P. Maldonado, F. Freimuth, A. Kronenberg, J. Henrizi, I. Radu, E. Beaurepaire, Y. Mokrousov, P. M. Oppeneer, M. Jourdan, G. Jakob, D. Turchinovich, L. M. Hayden, M. Wolf, M. Münzenberg, M. Kläui, and T. Kampfrath, Nat. Photonics **10**(7), 483 (2016).
[11]R. I. Herapath, S. M. Hornett, T. Seifert, G. Jakob, M. Kläui, J. Bertolotti, T. Kampfrath, and E. Hendry, Appl. Phys. Lett. **114**(4), 041107 (2019).
[12]O. Gueckstock, L. Nádvorník, T. S. Seifert, M. Borchert, G. Jakob, G. Schmidt, G. Woltersdorf, M. Kläui, M. Wolf, and T. Kampfrath, Optica **8**(7), 1013 (2021).
[13]M. Chen, Y. Wu, Y. Liu, K. Lee, X. Qiu, P. He, J. Yu, and H. Yang, Adv. Opt. Mater. **7**(4), 1801608 (2019).
[14]A. Leitenstorfer, A. S. Moskalenko, T. Kampfrath, J. Kono, E. Castro-Camus, K. Peng, N. Qureshi, D. Turchinovich, K. Tanaka, and A. G. Markelz, J. Phys. D **56**(22), 223001 (2023).
[15]S. Ito, M. Schüler, M. Meierhofer, S. Schlauderer, J. Freudenstein, J. Reimann, D. Afanasiev, K. Kokh, O. Tereshchenko, and J. Güdde, Nature **616**, 696–701 (2023).
[16]T. L. Cocker, V. Jelic, M. Gupta, S. J. Molesky, J. A. Burgess, G. D. L. Reyes, L. V. Titova, Y. Y. Tsui, M. R. Freeman, and F. A. Hegmann, Nat. Photonics **7**(8), 620 (2013).
[17]A. Sell, A. Leitenstorfer, and R. Huber, Opt. Lett. **33**(23), 2767 (2008).
[18]Q. Wu and X. C. Zhang, Appl. Phys. Lett. **67**(24), 3523 (1995).
[19]A. Leitenstorfer, S. Hunsche, J. Shah, M. C. Nuss, and W. H. Knox, Appl. Phys. Lett. **74**(11), 1516 (1999).
[20]T. S. Seifert, S. Jaiswal, J. Barker, S. T. Weber, I. Razdolski, J. Cramer, O. Gueckstock, S. F. Maehrlein, L. Nadvornik, S. Watanabe, C. Ciccarelli, A. Melnikov, G. Jakob, M. Münzenberg, S. T. B. Goennenwein, G. Woltersdorf, B. Rethfeld, P. W. Brouwer, M. Wolf, M. Kläui, and T. Kampfrath, Nat. Commun. **9**(1), 2899 (2018).
[21]J.-C. Diels and W. Rudolph, *Ultrashort Laser Pulse Phenomena* (Elsevier, 2006).
[22]L. Zhao, Z. Wang, C. Lu, R. Wang, C. Hu, P. Wang, J. Qi, T. Jiang, S. Liu, Z. Ma, F. Qi, P. Zhu, Y. Cheng, Z. Shi, Y. Shi, W. Song, X. Zhu, J. Shi, Y. Wang, L. Yan, L. Zhu, D. Xiang, and J. Zhang, Phys. Rev. X **8**(2), 021061 (2018).
[23]T. Cocker, V. Jelic, R. Hillenbrand, and F. Hegmann, Nat. Photonics **15**(8), 558 (2021).
[24]H. A. Hafez, S. Kovalev, J.-C. Deinert, Z. Mics, B. Green, N. Awari, M. Chen, S. Germanskiy, U. Lehnert, J. Teichert, Z. Wang, K.-J. Tielrooij, Z. Liu, Z. Chen, A. Narita, K. Müllen, M. Bonn, M. Gensch, and D. Turchinovich, Nature **561**(7724), 507 (2018).
[25]A. Alostaz, O. Gueckstock, J. Tong, J. Kredl, C. In, M. Münzenberg, C. Schneider, T. Kampfrath, and T. Seifert (2024). "Tunable ultrabroadband hybrid terahertz emitter combining a spintronic," Zenodo. https://zenodo.org/records/13936518